

Comparison of Whole-Body Kinematic Behaviour of the GHBMOC Occupant Model to PMHS in Far-Side Sled Tests

Maika Katagiri, Jay Zhao, Jason Kerrigan, Richard Kent, Jason Forman

Abstract Although far-side collisions have historically received little consideration in automotive safety, their fatality risk is comparable to that of near-side collisions. The future development of restraint systems for far-side protection requires a surrogate occupant model that could be used for a large number of iterative parametric studies. The goal of this study is to assess and enhance the biofidelity of the Global Human Body Model Consortium 50th percentile male occupant model (GHBMOC AM50-O v4.4) using 3D kinematics data from a series of post-mortem human subject (PMHS) far-side sled tests, which is the most comprehensive dataset currently available for biofidelity evaluation of human surrogates in far-side impacts. Since the PMHS in the sled tests exhibited significant lateral bending of the torso, mechanical properties of the spine of the human body model were re-examined using a series of cadaveric lumbar spine tests. Six PMHS far-side sled tests were modelled and simulated, which consisted of two low-severities with and without seatbelt pretensioning and one high-severity with pretensioning for oblique and lateral impact directions, respectively. The sensitivities of seatbelt pretensioning, impact severity and impact direction to occupant whole-body kinematic behaviour found in the PMHS tests were observed in the human body model simulations.

Keywords Far-side, human body model, lateral impact, oblique impact, spine.

I. INTRODUCTION

The crash mode of far-side collisions has historically not been addressed by crashworthiness evaluation and safety regulations or by consumer information ratings programs. With the most recent National Automotive Sample System (NASS) data, fatality risk in far-side collisions was found to be comparable that of in near-side collisions [1-2]. Oblique collisions were the most common impact direction among serious injuries in far-side collisions [3]. Head and thorax injuries, which accounted for more than half of serious injuries in far-side collisions, were attributed to contacts with far-side structures [1][3]. Also of concern are abdominal injuries, especially to the liver and spleen [4]. Recently, a series of far-side lateral and oblique sled tests with seven cadavers was conducted to investigate the effects of various restraint, positioning and collision parameters on occupant kinematics. In that study, Forman *et al.* [5] found that seatbelt pretensioning tended to increase the shoulder engagement, and an oblique impact direction tended to cause increased head lateral excursion and axial rotation of the torso.

The future design and optimisation of restraint systems for far-side protection requires a surrogate occupant model that could be used for a large number of iterative parametric studies. The Global Human Body Model Consortium 50th percentile male occupant model (GHBMOC AM50-O v4.4) could be a candidate for such applications. However, its biofidelity in far-side impact loading conditions needs to be further validated. Although the model was validated with a few sets of PMHS frontal and near-side sled tests, it has not been evaluated for far-side lateral and oblique collisions [6]. The PMHS far-side sled tests of Forman *et al.* [5] are so far the most comprehensive dataset available for the biofidelity evaluation of human surrogates in this impact condition. In addition, this modelling can be used to gain insight into how whole-body kinematic behaviour, especially the lateral and torsional motion of the torso, is affected by anthropometric, environmental and restraint parameters, as well as the stiffness of the spine.

M. Katagiri is a Research Engineer in Takata Corporation and TK Holdings Inc. (e-mail: Maika.Katagiri@Takata.com; tel: +1-248-475-6760) J. Zhao is a Technical Manager of the System Development Group in TK Holdings Inc.. J. Kerrigan is an Assistant Professor in the Department of Aerospace and Mechanical Engineering at University of Virginia. R. Kent is a Professor in Mechanical Engineering, Department of UVA, and Deputy Director of the University of Virginia Center for Applied Biomechanics. J. Forman is a Principal Scientist in Mechanical and Aerospace Engineering at UVA.

The goal of this study is to assess and enhance biofidelity of the GHBMC AM50-O v4.4 model using the 3D kinematics data from the PMHS far-side lateral and oblique sled tests [5], and also to obtain better understanding of the effects of anthropometric, environmental and restraint parameters on the whole-body kinematic behaviour, especially the lateral motion of the torso.

II. METHODS

To compare the GHBMC AM50-O v4.4 to the PMHS in far-side collisions, six PMHS far-side sled tests [5] were simulated, in which variations of impact severity, impact angle and seatbelt pretensioning were studied. Figure 1 shows the simulation model set-up to be run with the LS-DYNA v971 mpp 6.1.2. The whole-body kinematic behaviour was evaluated to observe the effects of the prescribed anthropometric, environmental, and restraint parameters.



Fig. 1. Far-Side Sled Test Simulation Model.

Computational Model of PMHS Far-Side Sled Test Environment

A detailed FE model of the sled and seat fixture was built based on the geometric data obtained from the test environment [5]. The local coordinate system of the seat fixture was defined to be the same as the tests, as shown in Fig. 2. A neoprene rubber layer on the top of the seat was modelled with solid elements with the rubber material property. A three-point seatbelt was modelled with a combination of 1D seatbelt elements and 2D membrane elements wrapped around the torso and abdomen with a fitting tool. One end of the shoulder-belt was connected to a retractor through a D-ring; the other end was connected to the lap-belt through the buckle. The retractor model reconstructed the functions of pretensioner and load limiter based on the force and the pay-in/-out of the seatbelt data recorded in the tests. The buckle arm model was deformable with a steel material property, with the buckle target matched to the trajectory measured from the pre-tests. A slip ring model was defined each for the D-ring and the Buckle. The seatback and footrest positions were adjustable so that the torso and feet regions of the human body model (HBM) were properly supported per the PMHS tests. The experimental crash pulse (lateral or oblique) from the far-side sled tests was applied as a prescribed motion to the whole seat fixture model in the directions shown in Fig. 2.

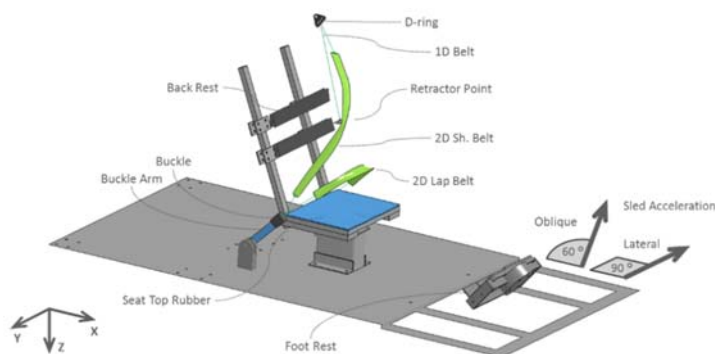


Fig. 2. Far-Side Sled Test Environment Model.

A parametric study was performed in the six PMHS test simulations to study the effects of variations of friction coefficients on the contact surfaces between the sled test model and HBM. The friction coefficients determined through this study were optimized to match the target traces of the pelvis CG, T7 and the ankle

displacements with that of the PMHS (quantified with Vicon 3D motion capture) throughout the six tests. The friction coefficients on the seat pan and the seatback were defined as 0.60 and 0.65 respectively. To achieve equivalent seatbelt forces and belt pay-in/-out to that of each PMHS test, the friction coefficient on the shoulder belt was 0.5 for the oblique and 0.8 for the lateral impact, and the lap belt friction coefficient was 0.5 for the oblique and 0.3 for the lateral impact.

Occupant Model and Validation of GHBMC AM50-O Spine Complex

The GHBMC AM50-O v4.4 model, developed by the Global Human Body Model Consortium [6], was used for this study. It represents a male occupant of 77 kg weight, 175 cm tall and BMI of 25.1, which are close to those of the PMHS simulated in this study (Table I). Compared to the HBM, the subject tested in the lateral impacts (PMHS-559) had a slightly leaner figure. Among the three PMHS tested in the oblique impacts, PMHS-602 had the closest body mass and stature to the model, and was therefore selected as the targeted subject used to position the HBM.

TABLE I
GHBMC OCCUPANT MODEL AND PMHS INFORMATION

	Mass [kg]	Stature [cm]	BMI	Age
GHBMC AM50-O	77	175	25.1	-
PMHS-559 (lateral)	73	175	23.8	60
PMHS-591 (oblique)	86	182	25.9	44
PMHS-602 (oblique)	79	178	24.9	61
PMHS-608 (oblique)	79	172	26.7	56

Our earlier study [7] using the GHBMC AM50-O v4.4 model to simulate the PMHS-559 in the far-side lateral sled tests indicated that the model exhibited stiffer spinal kinematics than the PMHS, who exhibited significant lateral bending of the thoracic and lumbar spine. In this study mechanical properties of the spine were re-examined using the lumbar spine test data of Demopoulos *et al.* [8]. Several major modifications to the model were made to improve its thoracic and lumbar spine biofidelity. First, a consistent joint modelling method for the whole thoracic and lumbar spine was applied. Original definitions of the spherical joints between each thoracic vertebra were changed to zero-length beam elements of six degrees of freedom (DoF), the same as the lumbar spine. The directions of local coordinate systems of the thoracic joints were also corrected to be consistent with the lumbar joints, as shown in Fig. 3. Secondly, the lumbar spine complex characteristics were calibrated with the cadaveric lumbar tests conducted by Demopoulos *et al.* [8]. Figure 4 shows the lumbar spine complex model set-up per Demopoulos’s cadaveric whole lumbar tests. Simulations were performed individually for each loading mode of compression, tension, anterior shear, posterior shear, lateral shear and lateral bending. The joint stiffness curves of the 6D zero-length beams were calibrated to the lumbar test measurements, averaged for the test subjects for each loading mode. As shown in Fig. 5, the original GHBMC AM50-O v4.4 model has a greater stiffness under the lateral shear and compression loading modes.

The modified occupant human model, named GHBMC AM50-O v4.4-MOD, was used in this study to conduct all the far-side sled test simulations.

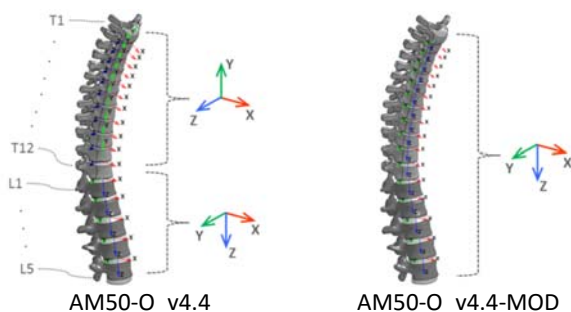


Fig. 3. Coordinate Systems of Spine Model.

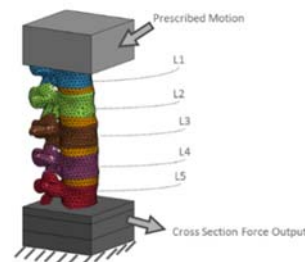


Fig. 4. Lumbar Spine Complex Validation Model.

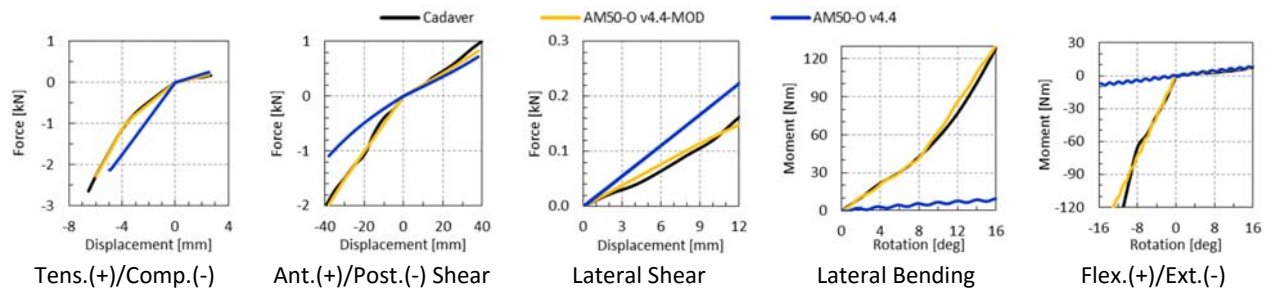


Fig. 5. Comparison of the whole lumbar spine responses: the models’ outputs vs. the test average curves [8].

The Far-Side Sled Simulation Matrix

Table II shows the far-side PMHS sled tests simulation matrix and corresponding PMHS information. The studied parameters were the impact direction, impact severity and seatbelt pretensioning. While these three parameters showed significant effect on subjects’ kinematic behaviour in the PMHS tests [5], significant effects of D-ring anterior-posterior position and upper extremity position were not observed. Three oblique (60°) and three lateral (90°) far-side impacts were simulated in this study. Each direction of impact consisted of two low-severity impacts (6.6 g) with and without seatbelt pretensioning, and one high-severity impact (14 g) with pretensioning. Among three different available D-ring anterior-posterior positions in the PMHS tests, the intermediate position was selected for all six simulations in this study. Each simulation case of the oblique impact corresponded to three PMHS tests, while each lateral impact simulation case corresponded to a single PMHS test.

TABLE II
MATRIX OF FAR-SIDE SLED SIMULATION AND CORRESPONDING PMHS TEST

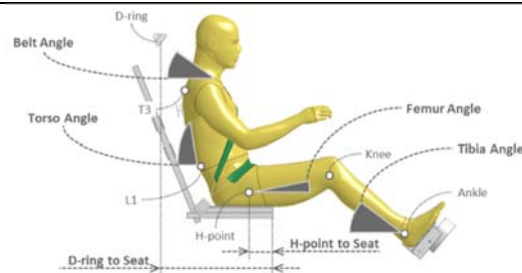
Case	Impact Direction	Sled Accel. [g]	Pretensioning	D-ring	PMHS Test #	PMHS #
133	Oblique (60°)	6.6	No	Intermediate	S0122	591
					S0133	602
					S0136	608
134	Oblique (60°)	6.6	Yes	Intermediate	S0123	591
					S0134	602
					S0137	608
135	Oblique (60°)	1.4	Yes	Intermediate	S0124	591
					S0135	602
089	Lateral (90°)	6.6	No	Intermediate	S0089	559
090	Lateral (90°)	6.6	Yes	Intermediate	S0090	
091	Lateral (90°)	14	Yes	Intermediate	S0091	

Initial Positions of GHBMC Occupant Model

The HBM was individually positioned to match the initial locations of head, torso, pelvis, knee and ankle targets of each PMHS in each test by performing a series of positioning pre-simulations. The lower limb and tibia were rotated around the hip joint and the knee joint respectively by a prescribed motion. To mimic the PMHS’s forward flexed neck/upper torso posture, the head/neck region of the HBM was rotated forward around T12. The buttocks and back of the torso were compressed to make a planar surface contacting to the seat and the back rest, respectively. Table III shows comparison of initial position between the HBM and the PMHS in terms of six position measurements in the sagittal plane: distance between H-point and the seat front edge; distance between D-ring to the seat front edge; angle between D-ring and left shoulder; angle between T3 and L1 (Torso Angle); angle between H-point and knee (Femur Angle); and angle between knee and ankle (Tibia Angle). The H-point to seat distance was different between the HBM and the PMHS, while other measurements were matched well. This was because matching H-point position was given a lower priority over matching the pelvis CG and head CG locations. Since the HBM’s torso region was difficult to position due to large numbers of parts and elements, the PMHS’s forward flexed torso (due to slouching) could not be achieved by the positioning pre-simulation method used in this study.

TABLE III
GHBM OCCUPANT MODEL AND PMHS INITIAL POSITION MEASUREMENTS

Case	HBM/PMHS	H-pt. to Seat [mm]	D-ring to Seat [mm]	Belt Angle [deg]	Torso Angle [deg]	Femur Angle [deg]	Tibia Angle [deg]
133	HBM	97	520	49	79	10	43
	PMHS-602	133	520	46	80	12	44
134	HBM	81	525	45	76	13	45
	PMHS-602	119	525	44	80	14	43
135	HBM	81	521	45	76	13	45
	PMHS-602	118	521	48	81	12	47
089	HBM	120	507	36	82	12	40
	PMHS-559	111	507	38	79	11	41
090	HBM	120	513	36	82	12	40
	PMHS-559	112	513	36	80	10	42
091	HBM	120	505	36	82	12	40
	PMHS-559	109	505	37	81	10	41



Analysis of Whole-Body Kinematic Behaviour

The whole-body kinematic behaviour of the HBM was compared to the PMHS test results by overlaying the time-histories of targets at head CG, T1, T7 and pelvis CG. For the PMHS tests, the kinematics were quantified using Vicon 3D motion capture to track bone-mounted marker array clusters, which were then transformed to calculate the motion of the specified bony landmarks [5]. Overall kinematics were further analysed by plotting each anatomical landmark (and the seatbelt path) in anterior, lateral and superior views in the seat reference frame at the time of maximum head excursion. As Fig. 6 shows, a stick-figure reconstruction of the body segments illustrates relative motion between each body region and interaction with seatbelt. In the PMHS tests, head CG, T1, left acromion, T4, T7, pelvis CG and left and right H-point targets were available for all impacts, and additional targets at L1 and L4 were available for the 90 degree lateral impacts.

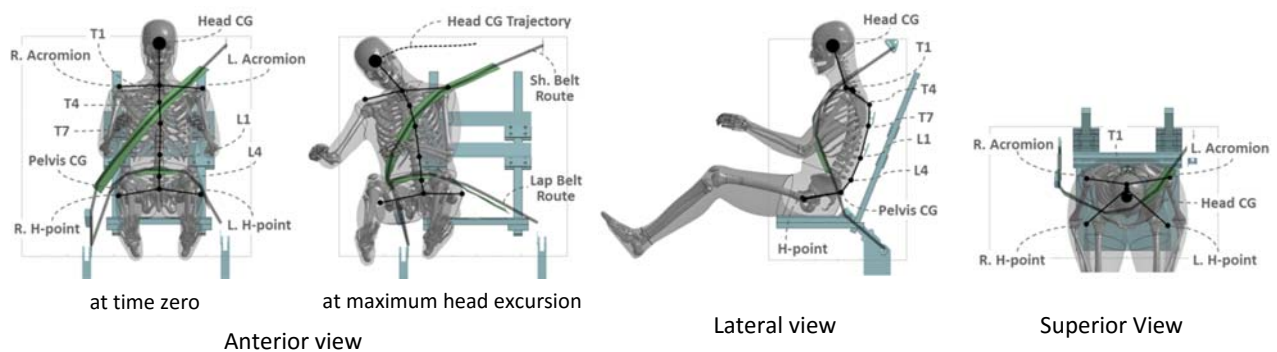


Fig. 6. Illustration of the stick-figure plots.

III. RESULTS

The time histories of the shoulder- and lap-belt force, belt pay-in/-out, displacement of head CG, T1, T7 and pelvis CG from the simulations were compared with those measured from the PMHS tests (Figs A1–A6, Appendix). Trend and magnitude of the shoulder and lap seatbelt forces and belt pay-in/-out were all within variation range of the measurements in all six simulations – except for the two cases of the low severity without seatbelt pretensioning (Case 133 and Case 089), where the lap-belt forces were slightly larger than the test data. The displacement of the HBM’s pelvis CG generally matched to that of the PMHS, with some deviations observed in the lateral displacement in Case 089 (6.6 g, 90°, No-Pretensioning) and in the longitudinal displacement in Case 091 (14 g, 90°, Pretensioning). The displacement of the HBM’s T7, which slid laterally between the two back-rest beams in the lateral impacts, was well matched until the point began to slide off from the back rest except Case 089.

Figure 7 shows the maximum lateral and longitudinal excursion of head CG during the simulations (150 ms) in the PMHS tests and the HBM simulations. Both in the PMHS tests and the HBM simulations, the head CG displacement increased along with the impact severity. Secondly, the lateral excursions in the oblique impacts were larger than those in lateral impacts, with the exception of the no-pretensioning case. Additionally, the head moved forward (positive in longitudinal) in the oblique impacts and backward (negative in longitudinal) in the lateral impacts. Furthermore, among the low severity lateral impacts, the head excursion was significantly decreased with the seatbelt pretensioning. Compared between the PMHS tests and the HBM simulations, the maximum displacement of the HBM head CG was larger than that of the PMHS except longitudinal displacement in the lateral impacts.

Overall kinematics comparisons are illustrated in plots at the time of the maximum head excursion shown in Figs 8–10 (oblique) and 11–13 (lateral). Tilting of pelvis (from left to right H-point via pelvis CG in the anterior view) shown in the oblique PMHS tests were not observed in the HBM simulations, while the z-axis rotation of the pelvis (from left to right H-point via pelvis CG in the superior view) in the lateral impacts was reconstructed well in the simulations. The PMHS torso tended to tilt laterally in the oblique impacts and to bend laterally in the lateral impacts, which were generally represented in the HBM simulations. The exception was the lower torso in Case 091. The trend of forward and lateral flexion of head-neck (from head CG to T1 CG) in the oblique impacts was observed in both the PMHS tests and the HBM simulations, while the magnitudes were different. The trend of lateral flexion of head-neck in the lateral impacts of the PMHS was well mimicked by the HBM among the three impacts. The left shoulder and seatbelt engagement in the PMHS oblique tests was observed in the HBM simulations, which resulted in similar belt routing over the torso. On the other hand, the PMHS’s shoulder partially slipped off the belt in the lateral impacts, except in Case 090 (6.6 g, 90°, Pretensioning), while the shoulder of HBM fully engaged with the seatbelt throughout the simulations (see Figs A4 and A6, Appendix).

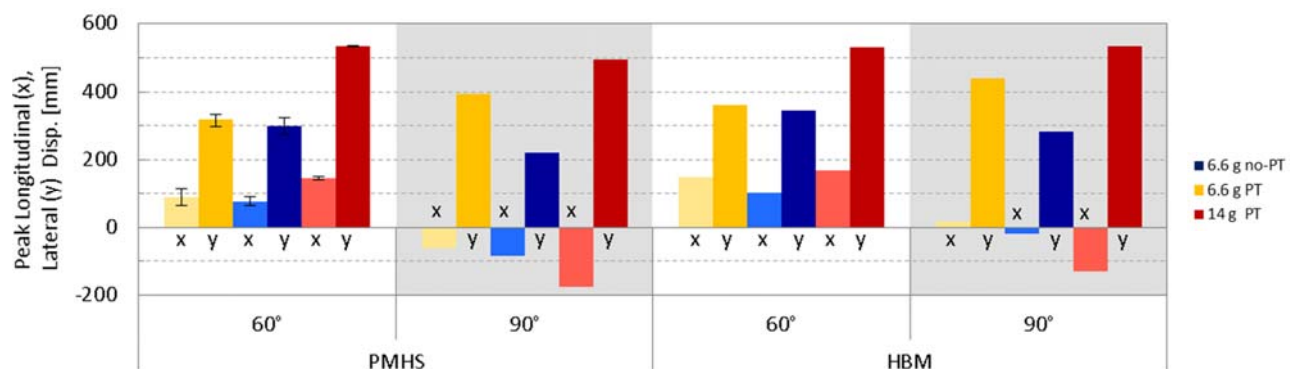


Fig. 7. Maximum displacement of head CG. In the PMHS oblique impact tests, the values and the error bars represent the average and the range among the subjects.

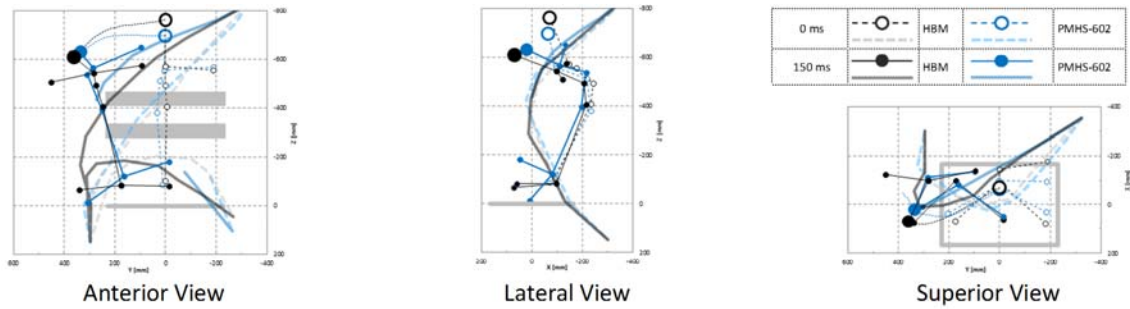


Fig. 8. Stick figure kinematics plots for Case 133 (6.6 g, 60°, No-Pretensioning) at the maximum head excursion.

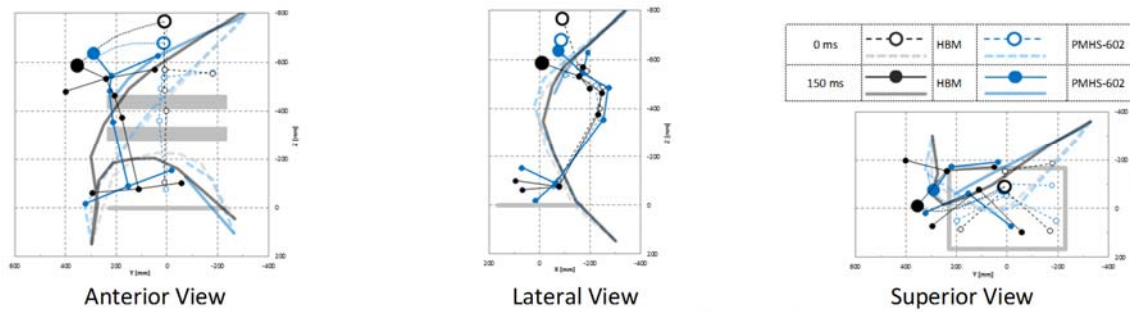


Fig. 9. Stick figure kinematics plots for Case 134 (6.6 g, 60°, Pretensioning) at the maximum head excursion.

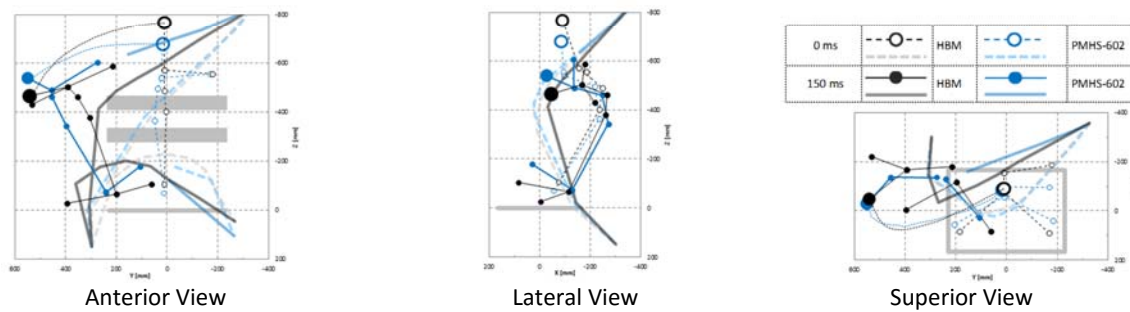


Fig. 10. Stick figure kinematics plots for Case 135 (14 g, 60°, Pretensioning) at the maximum head excursion.

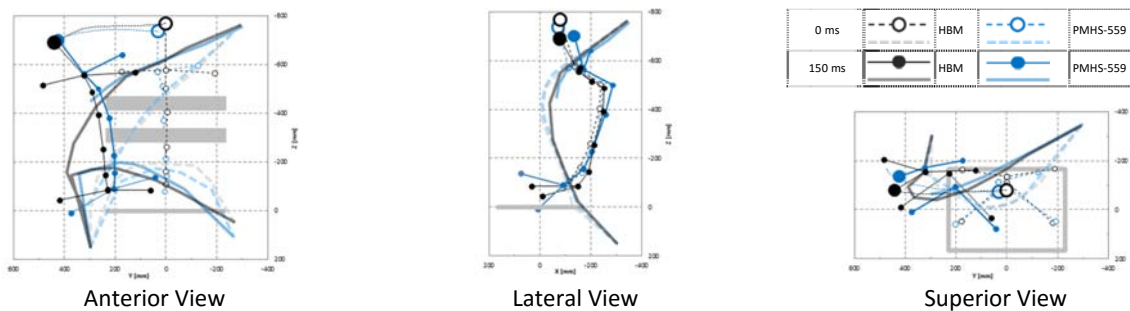


Fig. 11. Stick figure kinematics plots for Case 089 (6.6 g, 90°, No-Pretensioning) at the maximum head excursion.

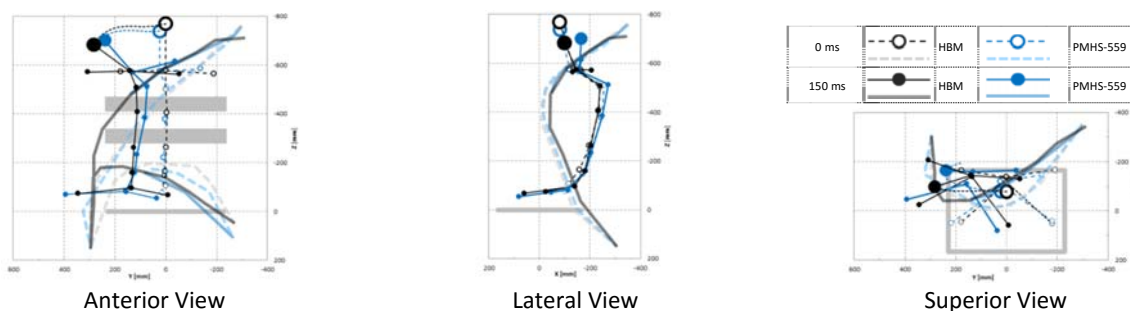


Fig. 12. Stick figure kinematics plots for Case 090 (6.6 g, 90°, Pretensioning) at the maximum head excursion.

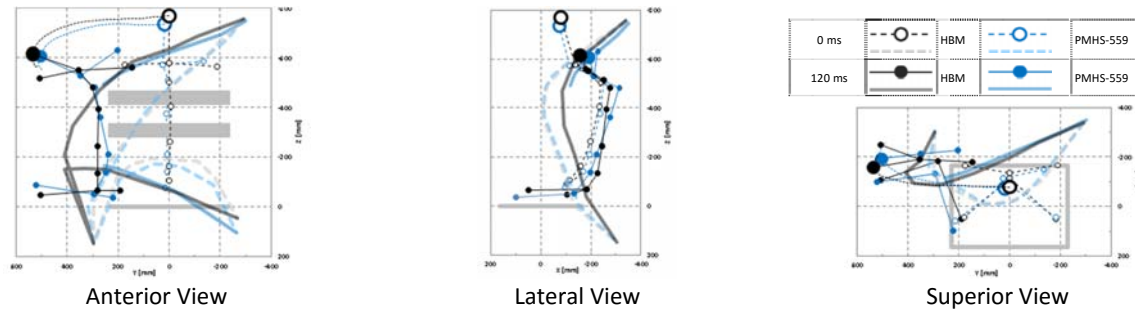


Fig. 13. Stick figure kinematics plots for Case 091 (14 g, 90°, Pretensioning) at the maximum head excursion.

IV. DISCUSSION

The results of seatbelt force, belt payout and displacement of pelvis CG and T7 indicated that the far-side sled test simulations in this study using the HBM reconstructed the PMHS tests reasonably well. The seatbelt force and belt payout matched to those from the tests in both trend and magnitude, which meant that the external force applied by the seatbelt was well mimicked. The consistency of the pelvis displacement also suggests that the material and contact friction of the seat were reasonably modelled. In the 90 degree lateral impacts (where the occupants' torso back remained in contact and slid along the back rest), the consistency of the T7 displacement suggests that the friction with the back rest was also appropriately represented.

The sensitivities to seatbelt pretensioning, impact severity and impact direction on the occupant kinematics that were found in the PMHS tests were also observed in the HBM simulations. General consistency in the torso kinematics and belt forces suggests that the modified mechanical properties of HBM spine represented the PMHS spine reasonably well in the simulations. While the HBM lumbar spine complex was calibrated to the cadaveric test [8] in multiple loading modes, validation of the spine in a full-body model simulation with cadaveric tests such as those conducted by McGill *et al.* [9] might lead further understanding of its biofidelity. Further evaluations, especially the assessment of injuries, are required if it is to serve as an accurate tool for restraint evaluation and injury prediction.

There are some variations in the sled test model, which might cause differences or deviations of the simulation results compared to the tests. First, while the HBM and the PMHS had approximately 50th percentile anthropometry and similar BMI, the PMHS's pelvis region was generally larger and rounder than the HBM's pelvis, and the abdomen shapes of the HBM were different from the tested PMHS. Such localised anthropometric difference could affect the seatbelt routing and may have contributed to the deviation of pelvis y-axis rotation in the oblique impacts. Secondly, the HBM's solid elements around the pelvis and shoulder behaved somewhat stiffer than would be expected with the superficial softer tissues of the PMHS. In that context, future work should include extended validation material properties of the HBM's superficial tissues (e.g. skin, fat, superficial musculature) in order to ensure proper interaction with the belt. Thirdly, the difference of initial location of T1 and its geometrical relation with head CG may have caused some differences in magnitude of head-neck forward and lateral flexion. Lastly, as shown in Table I, the subject tested in the lateral impacts (PMHS-559) was slightly leaner than the HBM. Effect of such a leaner stature tends to make difference between the PMHS and the HBM of the seatbelt routings relative to the neck, although the belt routing traces respect to the sled fixture were same. For the PMHS the shoulder-belt initially routed near the left acromion due to his narrower torso, while for the HBM the seatbelt routed closer to the neck, as shown in Figs 11 and 12. This could have contributed to the differences in shoulder-to-belt engagement with the HBM compared to the PMHS for those test conditions.

V. CONCLUSIONS

The modified version of GHBM 50th percentile male occupant model (GHBM AM50-O v4.4-MOD) from this study demonstrated reasonably well biofidelic kinematic responses in the six simulated PMHS test configurations. The updated HBM showed whole-body kinematic behaviour sensitivity to the studied parameters of seatbelt pretensioning, impact severity and impact direction to occupant kinematics that was

consistent with the trends observed in the PMHS tests. Further investigation and the model validations could be made toward improvement of a precise positioning tool and material properties calibration for the connective soft tissues, especially in the abdomen and pelvis regions.

VI. ACKNOWLEDGEMENTS

The authors gratefully acknowledged Scott Gayzik, an assistant professor in Wake Forest University School of Medicine, who has been the Principal Investigator of GHBMC Full Body Model Centers of Expertise, for his support in providing the baseline GHBMC AM50-O v4.4 model and his valuable comments on possible modifications to the model. Jialou Hu at Takata assisted in construction of the human lumbar model set-up per Demetropoulous's cadaveric lumbar spine tests.

VII. REFERENCES

- [1] Gabler, H. C., Fitzharris, M., Scully, J., Fildes, B. N. Far side impact injury risk for belted occupants in Australia and the United States. *Proceedings of the 19th International Technical Conference on the Enhanced Safety of Vehicles*, 2005, Washington D.C., 05-0420.
- [2] Pintar, F. A., Yoganandan, N., et al. (2007) Comparison of PMHS, WorldSID, and THOR-NT responses in simulated far side impact. *Stapp Car Crash Journal*, **51**: pp.313–60.
- [3] Bahous, G., Murakhovskiy, D., Digges, K., Rist, H., Wiik, R. Opportunities for reducing far-side casualties. *Proceedings of the 23rd International Technical Conference on the Enhanced Safety of Vehicles*, 2015, Gothenburg, Sweden, 15-0444.
- [4] Yoganandan, N., Pintar, F. A., Gennarelli, T. A., Maltese, M. R. (2000) Patterns of abdominal injuries in frontal and side impacts. *Annual Proceedings of the Association for the Advancement of Automotive Medicine*, **44**: pp.17–36.
- [5] Forman, J., Lopez-Valdes, F., et al. (2013) Occupant kinematics and shoulder belt retention in far-side lateral and oblique collisions: a parametric study. *Stapp Car Crash Journal*, **57**: pp.343–85.
- [6] GHBMC AM50-O v4.4 User's Manual. *Global Human Body Model Consortium*, 2015.
- [7] Katagiri, M., Zhao, J., Wiik, R. Parametric study for far side occupant protection using GHBMC Human Body Model. *SAE 2016 Government/Industry Meeting*, Washington, D.C., G105.
- [8] Demetropoulous, C., Yang, K., Grimm, M., Khalil, T., King, A. (1998) Mechanical properties of the cadaveric and Hybrid III Lumbar Spines. *Stapp Car Crash Journal*, **42**: pp.337–46.
- [9] McGill, S., Seguin, J., Bennett, G. (1994) Passive stiffness of the lumbar torso in flexion, extension, lateral bending, and axial rotation: Effect of belt wearing and breath holding. *Spine*, **19**(6): pp.696–704.

APPENDIX

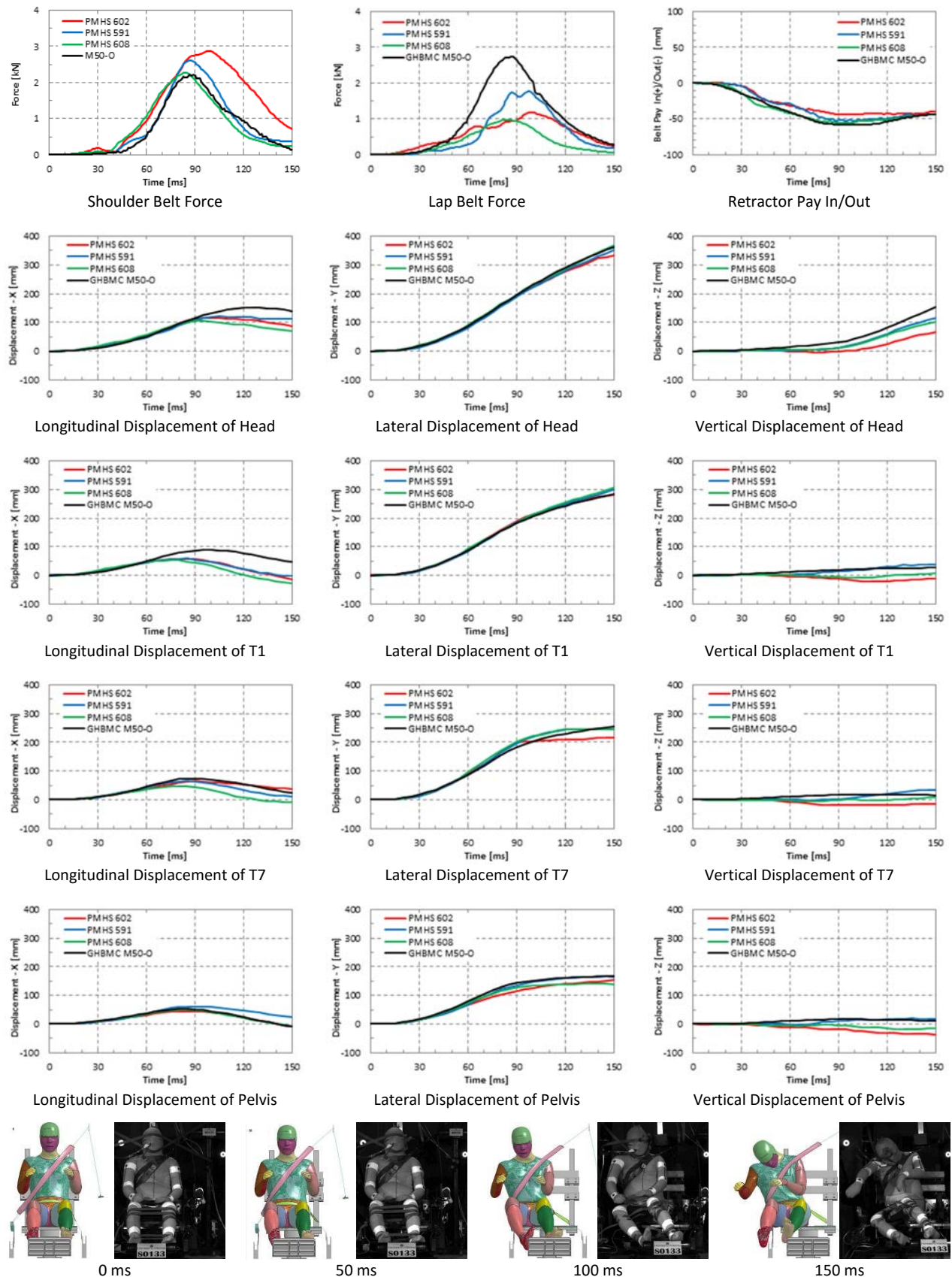


Fig. A1. Case 133 (6.6 g, 60°, No-Pretensioning)

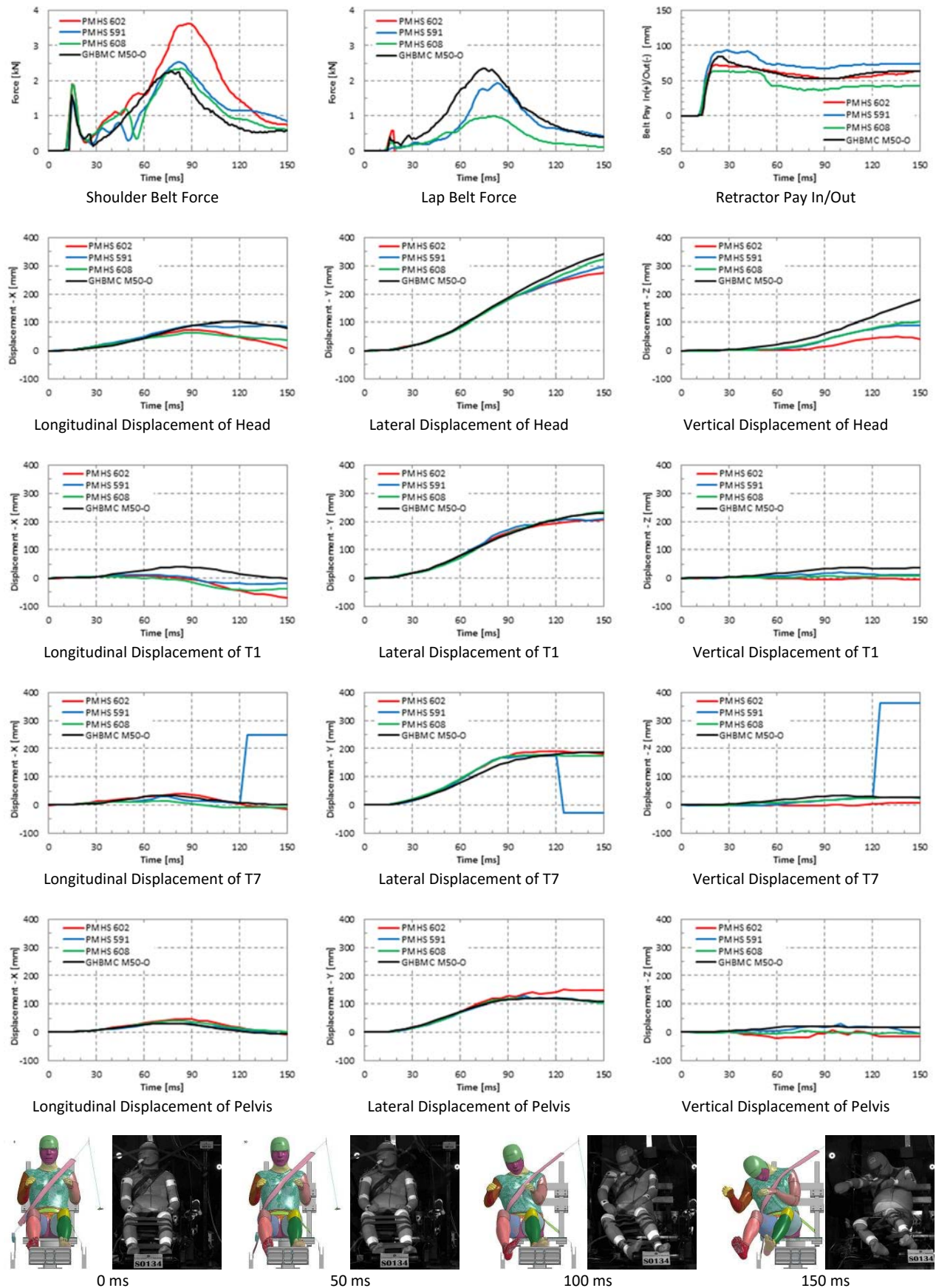


Fig. A2. Case 134 (6.6 g, 60°, Pretensioning)

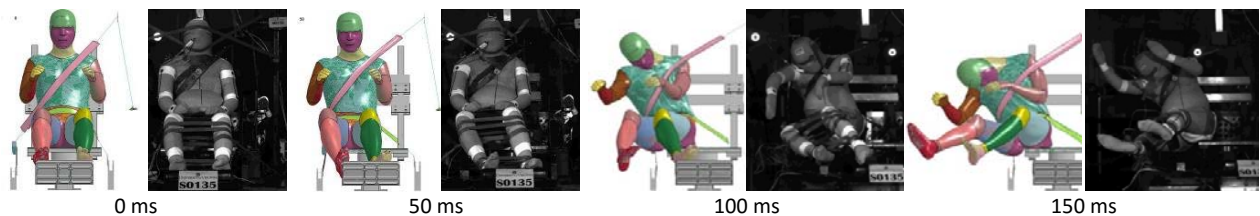
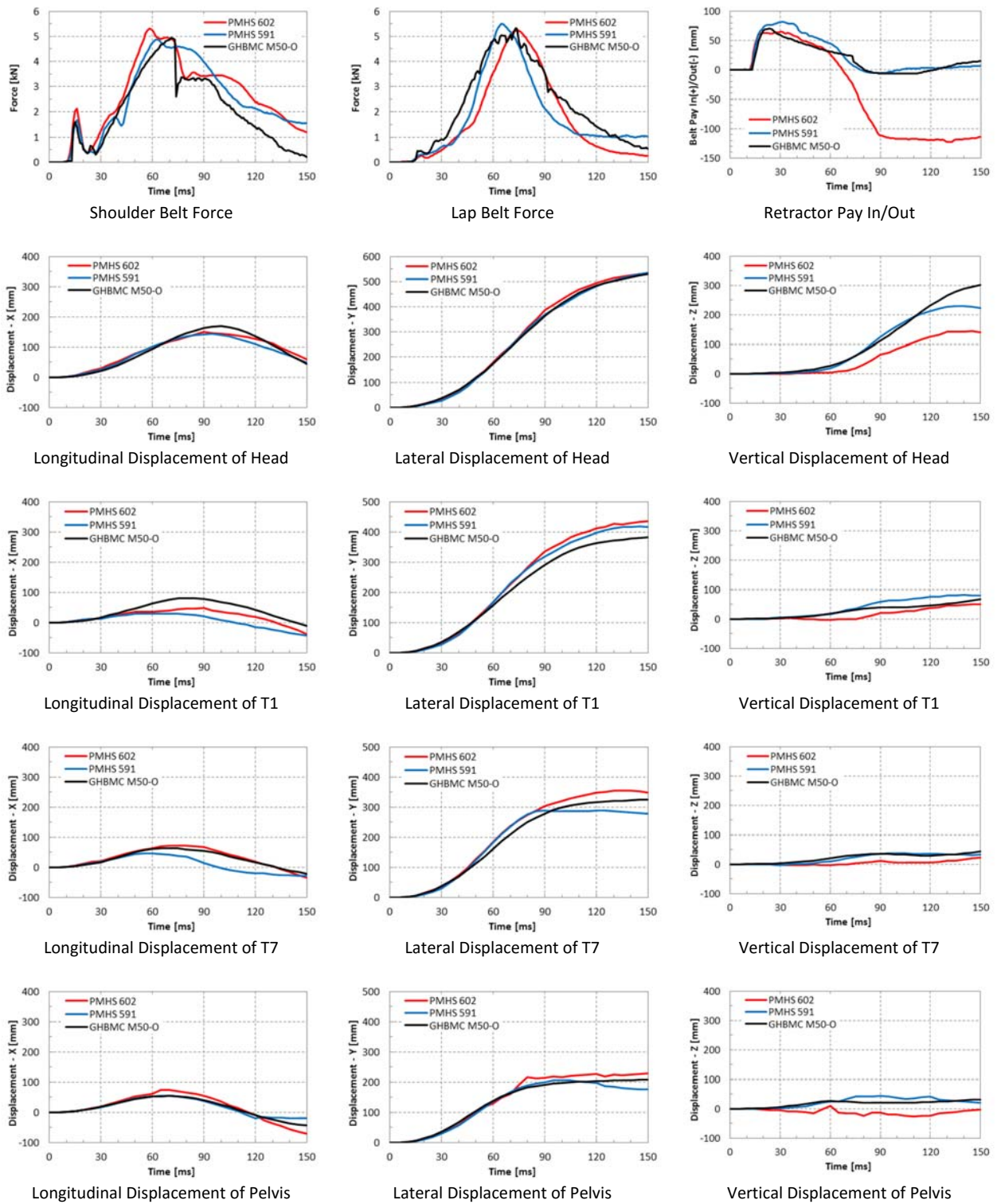


Fig. A3. Case 135 (14 g, 60°, Pretensioning)

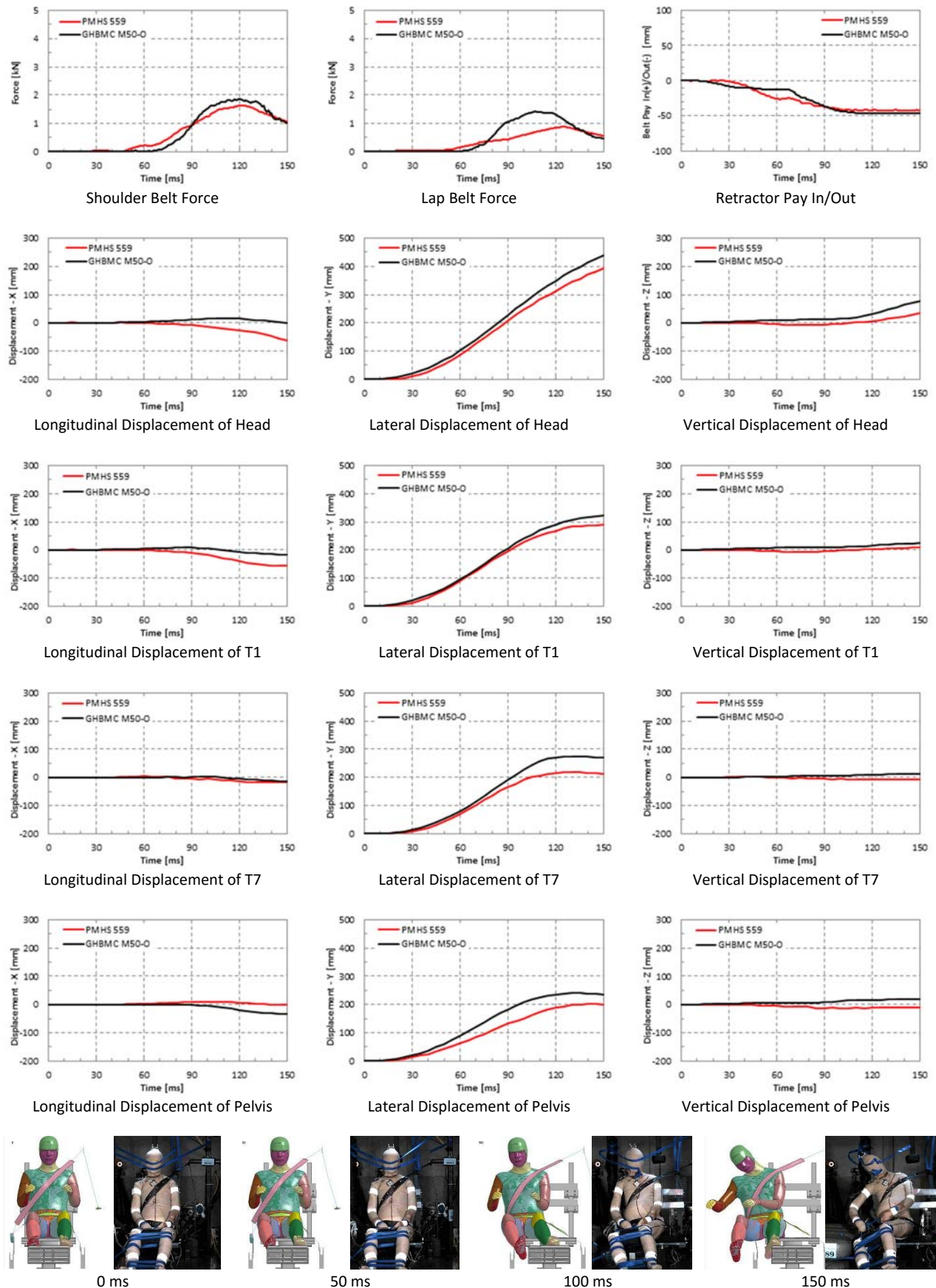


Fig. A4. Case 089 (6.6 g, 90°, No Pretensioning)

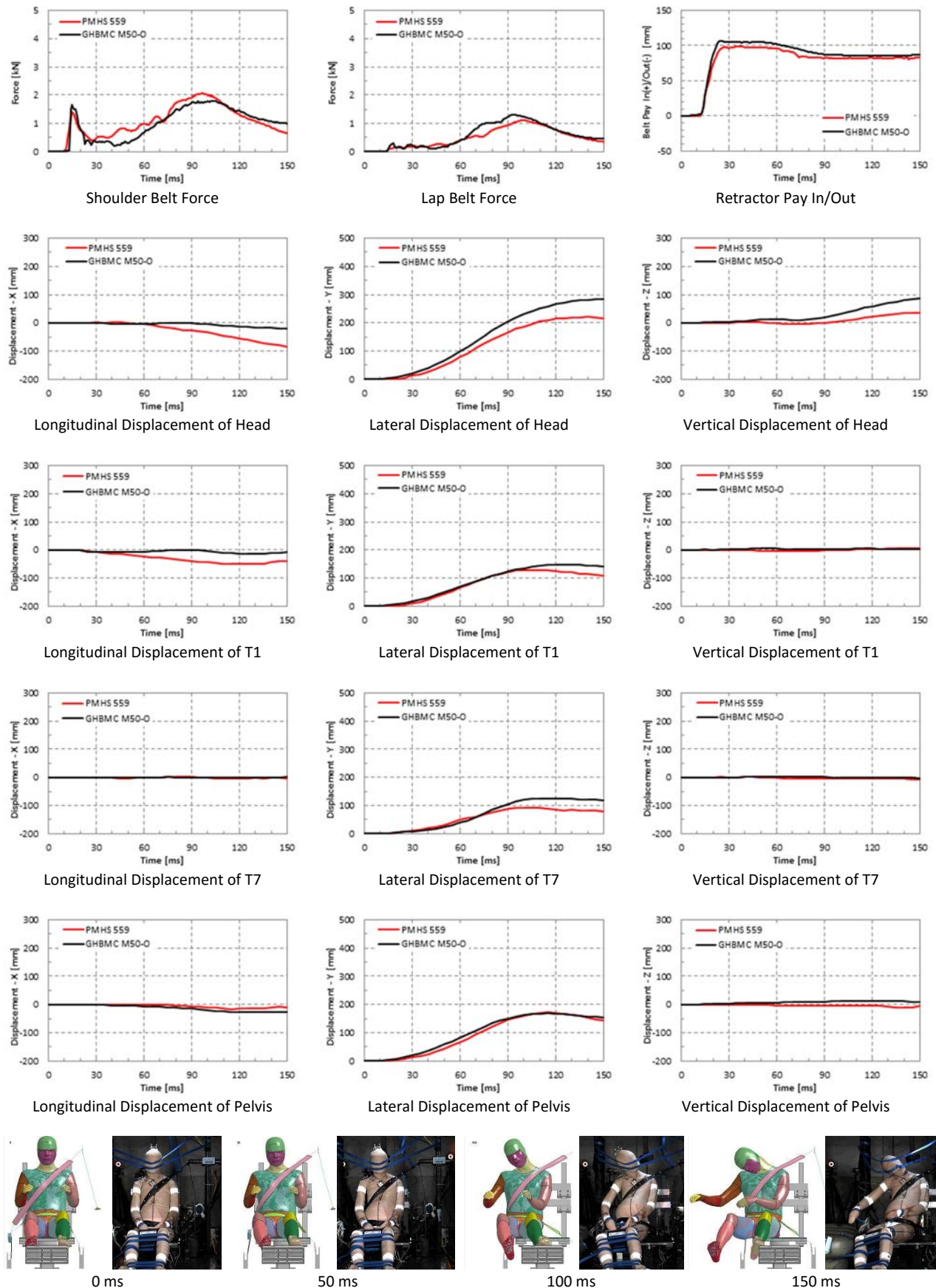


Fig. A5. Case 090 (6.6 g, 90°, Pretensioning)

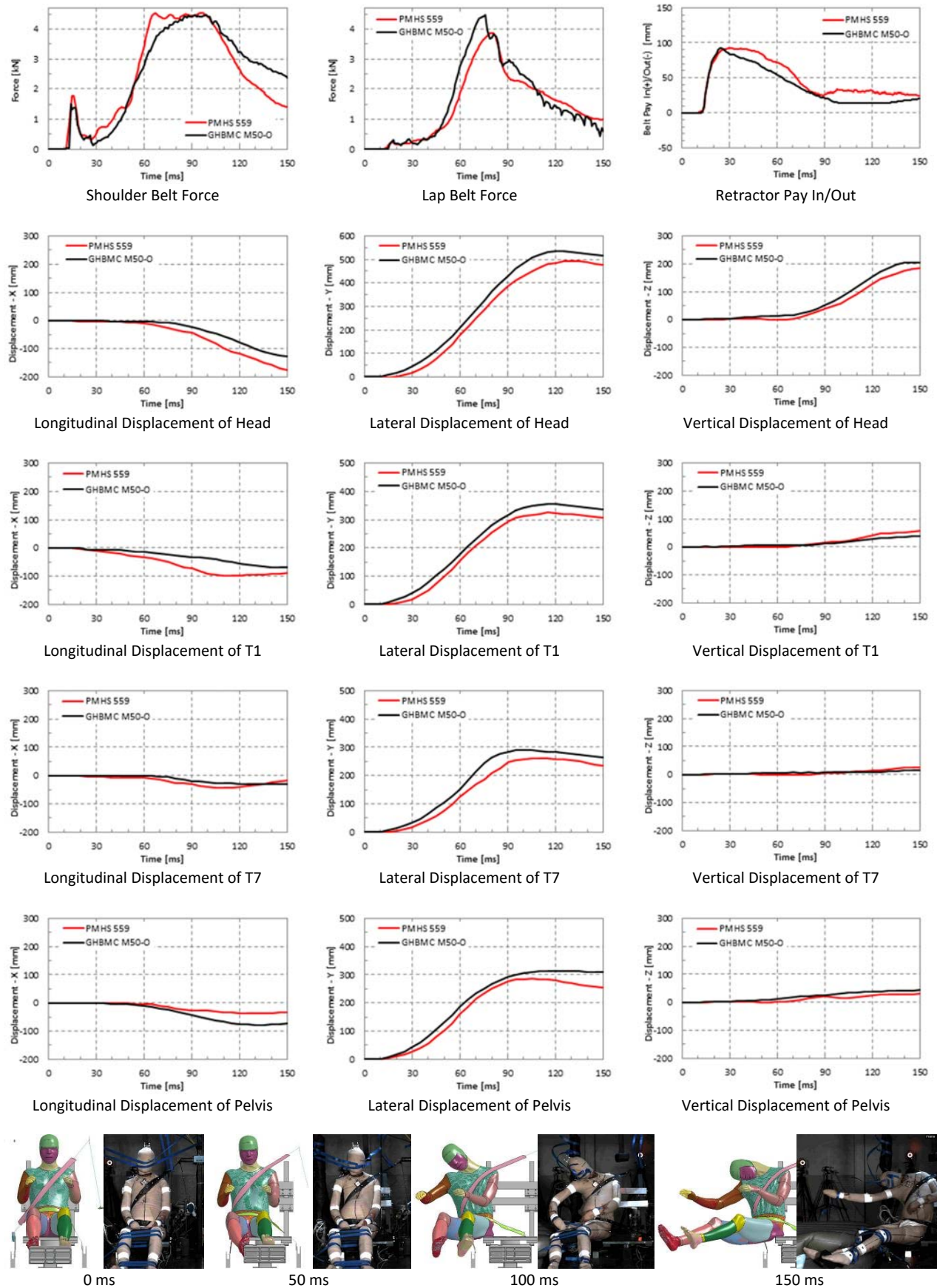


Fig. A6. Case 091 (14 g, 60°, Pretensioning)